Recombinant production of A1S_0222 from *Acinetobacter baumannii* ATCC 17978 and confirmation of its DNA-(adenine N6)-methyltransferase activity

Ulrike Blaschke [a], Beneditta Suwono [a], Sachli Zafari [b], Ingo Ebersberger [b,c], Evelyn Skiebe [a], Cy. M. Jeffries [d], Dmitri I. Svergun [d] and Gottfried Wilharm [a]*

[a] Robert Koch-Institute, Project group P2, Wernigerode, Germany

[b] Applied Bioinformatics Group, Institute of Cell Biology and Neuroscience, Goethe University, Frankfurt/Main, Germany

[c] Senckenberg Biodiversity and Climate Research Centre Frankfurt (BIK-F), Frankfurt/Main, Germany

[d] European Molecular Biology Laboratory (EMBL) Hamburg Outstation, 22607 Hamburg, Germany

* Corresponding address: Gottfried Wilharm, Robert Koch-Institut, Bereich Wernigerode, Burgstr. 37, D-38855 Wernigerode, Germany, e-mail: wilharmg@rki.de, Phone: +49 30 18754 4282; Fax: +49 30 18754 4207

Abstract

Acinetobacter baumannii appears as an often multidrug-resistant nosocomial pathogen in hospitals worldwide. Its remarkable persistence in the hospital environment is probably due to intrinsic and acquired resistance to disinfectants and antibiotics, tolerance to desiccation stress, capability to form biofilms, and is possibly facilitated by surface-associated motility. Our attempts to elucidate surface-associated motility in *A. baumannii* revealed a mutant inactivated in a putative DNA-(adenine N6)-methyltransferase, designated A1S_0222 in strain ATCC 17978. We recombinantly produced A1S_0222 as a glutathione S-transferase (GST) fusion protein and purified it to near homogeneity through a combination of GST affinity chromatography, cation exchange chromatography and PD-10 desalting column. Furthermore we demonstrate A1S_0222-dependent adenine methylation at a GAATTC site. We propose the name AamA (*Acinetobacter* adenine

methyltransferase A) in addition to the formal names M.AbaBGORF222P/M.Aba17978ORF8565P. Small angle X-ray scattering (SAXS) revealed that the protein is monomeric and has an extended and likely two-domain shape in solution.

Keywords: *Acinetobacter baumannii*, DNA-adenine-methyltransferase, epigenetic, recombinant, *E.coli*, AamA, M.AbaBGORF222P

Highlights

- First purification of a m6A DNA methyltransferase from *Acinetobacter baumannii* (AamA)
- Verification of methyltransferase activity of AamA *in vitro*
- Monomeric structure of AamA confirmed by SAXS
- AamA is ubiquitously present in *Acinetobacter* spp.

Abbreviations

SAXS, small angle X-ray scattering; DESY, Deutsches Elektronen-Synchroton; GST, glutathione S-transferase; m6A, methylation of the adenosine base at the nitrogen-6 position

Introduction

Acinetobacter baumannii is a gram-negative opportunistic pathogen that causes nosocomial infections including pneumonia and bloodstream infections which is associated with an increased mortality and multi-drug resistance [1-3]. *A. baumannii* was rated as one of the critical priority 1 pathogens for the development of new antibiotics by the WHO in 2017 [4].

Despite the name “Acinetobacter” meaning non-motile bacteria and despite the lack of flagella, members of the genus are able to move [5, 6]. At least two forms of motility are known for *Acinetobacter* species. The so called “twitching motility” depends on retraction of type IV pili [7-9]. Another form of movement, the surface-

associated motility, occurs at the surface of semi-dry media and is independent of type IV pili [10]. Almost all tested clinical isolates can move along surfaces [11] and a number of genes required for this form of motility have been identified [10, 12, 13].

Motility is known to be affected by epigenetic regulation in various bacteria [14]. Epigenetics deals with heritable changes in gene expression without any changes in the DNA sequence. In bacteria the most studied epigenetic mechanism is DNA methylation [15] that is performed by DNA methyltransferases [16]. These enzymes transfer methyl groups from S-adenosyl-L-methionine (SAM) to adenine or cytosine bases. This process protects DNA against digestion from restriction endonucleases and is important for the regulation of various physiological processes such as mismatch repair and transcription [17, 18]. Most DNA methyltransferases are part of a restriction-modification system (R-M system). In this case the host DNA gets methylated by the DNA methyltransferase that protects the DNA against digestion by the corresponding endonuclease [19]. In addition, “orphan” methyltransferases are known that act without any associated endonuclease [17]. The most studied orphan DNA adenine methyltransferase called Dam was found in *E. coli* and was shown to methylate adenine bases at GATC sites [20, 21]. *Salmonella enterica dam* mutants exhibit a reduced motility [22] and *dam* overexpression in *Yersinia enterocolitica* resulted in an increased motility [23].

The *Acinetobacter baumannii* genome encodes a putative DNA-(adenine N6)-methyltransferase, designated A1S_0222 in strain ATCC 17978 that seems to act without a corresponding endonuclease. We hypothesized that the putative DNA adenine methyltransferase A1S_0222 does impose epigenetic control in *Acinetobacter baumannii* and since little is known about orphan methyltransferases we approached its characterization.

Materials and Methods

Bacterial transformation and the generation of a *A. baumannii* ATCC 17978 mutant. Transformation was performed by electroporation [24]. The EZ-Tn5™ <KAN-2> transposon mutants in *A. baumannii* ATCC 17978 were generated by using the EZ-Tn5™ <KAN-2> insertion kit (Epicentre Biotechnologies) as previously described [11].

Surface-associated motility. Motility plates were composed of 0.5% agarose (w/v), 5 g/L of tryptone, and 2.5 g/L of NaCl as previously described [11]. A single colony from a nutrient agar plate (Oxoid) or selective agar plates (supplemented with 50 µg/mL of kanamycin for the A1S_0222 mutant) of either wild-type or *A. baumannii* ATCC 17978 mutant was taken with the pipette tip and then the surface of a motility plate was touched. Pictures were taken after incubating the plates for 16 h at 37°C.

Construction of protein expression plasmids. The *a1s_0222* gene of *A. baumannii* ATCC 17978 was amplified by PCR using the oligonucleotides *0222-pGEX-6P-3-for*: 5'-ATTAGGATCCAATTCAGAGCCTTCGGTATACCAC-3' (BamHI restriction site underlined) and *0222-pGEX-6P-3-rev*: 5'-ATTAGCGGCCGCTTACCAAAGTGCGAGCTGTGTAC-3' (NotI restriction site underlined). The amplified *a1s_0222* gene was inserted into pGEX-6P-3 expression vector (GE Healthcare) after digestion of insert and vector with BamHI and NotI restriction enzymes. The pGEX-6P-3 expression vector carries a glutathione S-transferase (GST-tag) gene, a PreScission protease restriction site, an ampicillin resistance (Amp^R) cassette, encodes a *tac* promotor and is inducible with isopropyl β-D-1-thiogalactopyranoside (IPTG). The plasmid (pGEX-6P-3-A1S_0222) was confirmed by DNA sequencing and transformed into *E. coli* BL21 (DE3) pLysS expression strain.

Protein expression and purification. A 3 mL overnight culture of *E. coli* BL21 (DE3) pLysS pGEX-6P-3-A1S_0222 was grown in Luria-Bertani (LB)-Medium (10 g/L tryptone, 5 g/L yeast extract, 5 g/L NaCl, pH 7.4, 100 µg/mL Amp) at 37°C and 160 rpm. The overnight culture was diluted 1:100 into 200 mL LB (supplemented with 100 µg/mL Amp) and cultured in a 2 L bottle-flask at 20°C and 160 rpm for 5 hours. Expression was induced by addition of 0.05 mM IPTG and cultures were incubated for 16 h at 20°C and 160 rpm. Cells were then harvested by centrifugation (10,000 × *g* for 30 min at 4°C) and the resulting cell pellets were frozen at -80°C. Cell pellets were solubilized at 4°C in 20 mL disruption buffer (300 mM NaCl, 1 mM DTT (1,4-dithiothreitol), 5 mM EGTA (ethylene glycol-bis(2-aminoethylether)-N,N,N′,N′-tetraacetic acid), 1 mM EDTA (2,2',2'',2'''-(ethane-1,2-diyldinitrilo) tetraacetic acid), 2 µL benzonase nuclease (250 U/µL), pH 7.4. The cells were lysed by applying three passages through an EmulsiFlex-C3 homogenizer (Avestin). Lysates were then

centrifuged at 20,000 × *g* for 50 min at 4°C. The soluble lysate was then added to a GSTPrep™ FF 16/10 column (GE Healthcare Life Sciences).

GST affinity chromatography. The GSTPrep™ FF 16/10 column (bed volume 20 mL) was equilibrated with 5 column volumes (CV) of GST binding buffer (300 mM NaCl, 1 mM DTT, 5 mM EGTA, 1 mM EDTA, 5% glycerol (v/v), pH 7.4). The soluble lysate was added to the column and washed with 10 CV of GST binding buffer and eluted with 7 CV of GST elution buffer (300 mM NaCl, 50 mM Tris, 1 mM DTT, 5 mM EGTA, 1 mM EDTA, 5% glycerol (v/v), 10 mM reduced L-glutathione (GSH reduced), pH 7.4). Eluted fractions were analyzed by SDS-PAGE and appropriate fractions were pooled. The GST fusion protein was then incubated for 16 h at 8°C with 40 units PreScission protease per 14.52 mg recombinant A1S_0222 to cleave off the GST tag (26 kDa). After incubation the pooled fractions were centrifuged at 20,000 g for 20 min at 4°C and diluted 1:4 in dilution buffer (50 mM Tris, 1 mM EDTA, 1 mM DTT, 5% glycerol (v/v)).

Cation exchange chromatography (CEC). The HiTrap™ SP XL (GE Healthcare Life Sciences) column (bed volume 1 mL) was equilibrated with 10 column volumes (CV) CEC binding buffer (50 mM NaCl, 50 mM Tris, 1 mM DTT, 1 mM EDTA, 5% glycerol (v/v)). The protein solution was loaded on the column and the column washed with 5 CV CEC binding buffer and subsequently eluted with 30 CV in a linear gradient from 0% to 100% of CEC elution buffer (1000 mM NaCl, 50 mM Tris, 1 mM DTT, 1 mM EDTA, 5% glycerol (v/v)). Eluted fractions were analyzed by reducing sodium dodecyl sulfate polyacrylamide gel electrophoresis (SDS-PAGE), pooled and loaded on a PD-10 desalting column.

PD-10 desalting column. The PD-10 desalting (GE Healthcare Life Sciences) column was equilibrated with buffer B1. Further steps were performed as described in the column manual using a gravity desalting protocol. The A1S_0222 protein was eluted with buffer B1 (150 mM NaCl, 10 mM Tris, 1 mM DTT and 5% glycerol (v/v), pH 7.4). Pooled fractions were concentrated using the Vivaspin® concentrator with a molecular weight cutoff of 10,000 Dalton and a Hydrosart (HY) membrane (Sartorius Stedim Biotech). The purity of A1S_0222 was analyzed by reducing SDS-PAGE. Protein concentrations were determined using the Bradford method. Purified A1S_0222 was directly used for further analysis or stored at -80°C.

Confirmation of the A1S_0222 DNA methylation recognition site. To confirm the A1S_0222 DNA methylation recognition site, the 800 base-pair (bp) PCR product, Int1, consisting of the 5'-end of the *a1s_0222* gene from *A. baumannii* ATCC 17978, was incubated with and without purified A1S_0222 at 37°C for one hour (3 µL Int1 (about 200 ng/µL), 2 µL B1 buffer, 4 µL of 800 µM S-adenosyl-L-methionine (SAM), 3 µL A1S_0222 (2.46 µg/µL), 8 µL RNase free water). Int1 was amplified with the oligonucleotides *Int1-for*: 5'-GGATCCGGATGAAATGATCAGTTATGTGGC-3' and *Int1-rev*: 5'-CGCTCTAATGCTGTTTGTGTACG-3'. Samples of methylated and non-methylated Int1 DNA were used for Sanger DNA sequencing and analyzed at the Robert Koch-Institute sequencing lab (Berlin, Germany) on an ABI PRISM analyzer. The sequencing chromatograms were analyzed as described previously [25].

DNA methylation assay. To test the biological activity of purified A1S_0222, a methylation assay was performed using the Int1 DNA. As an alternative DNA substrate, Seq3 (located in gene A1S_0965 of *A. baumannii* ATCC 17978) was amplified from *Acinetobacter baumannii* 29D2 using the oligonucleotides *Seq3-for*: 5'-GAAGTCACTGATACCAAGGAAGGTATTCATTTTG-3' and *Seq3-rev*: 5'-GTCTGGAAAATGCTGTGTTTCTAATGCTAG-3' (801 bp). Each fragment contains one *EcoR*I restriction site (G↓AATTC). For the methylation reaction 1 µg of Int1 or Seq3, 2 µL B1 buffer, 4 µL of 800 µM SAM, 8 µL RNase free water and 3 µL A1S_0222 (2.46 µg/µL) or 40 units EcoRI methyltransferase (New England BioLabs) were mixed and incubated for up to one hour at 37°C. After incubation A1S_0222 or EcoRI methyltransferase was inactivated by 95°C for 5 minutes and Int1 or Seq3 were purified with Hi Yield® Gel/PCR DNA Fragment Extraction Kit (SLG®) according to the manufacturer's instructions and eluted in 10 µL RNase free water. Subsequently, an EcoRI restriction reaction was performed (5 µL purified Int1 or Seq3, 1 µL EcoRI, 2 µL EcoRI buffer, 12 µL RNase free water) for 2 hours at 37°C. For visualization, agarose electrophoresis was carried out at 110 V for 50 min in TAE buffer (agarose concentration: 1.25% (w/v)). GelRed™ (GeneON) was used for gel staining. GelRed™ stock solution was diluted 1:5000 into the agarose gel solution. As a size standard GeneRuler DNA Ladder Mix (Thermo Fisher Scientific) was used. The methyltransferase activity was calculated based on the definition that 1 unit (U) of enzyme converts 1 µmol of substrate per minute at 37°C.

Small angle X-ray scattering (SAXS). Synchrotron SAXS measurements ($I(s)$ vs s, where $s = 4\pi\sin\theta/\lambda$; 2θ is the scattering angle and λ=0.125 nm) were performed at the EMBL-P12 bioSAXS beam line at the PETRA III storage ring (DESY, Hamburg) as described in [26] under continuous-flow batch mode operations at 10°C utilizing an automated robotic sample changer [27]. The scattering intensity data were recorded from 25 μl aliquots of A1S_0222 (2.4 mg/mL) and a corresponding matched solvent blank (150 mM NaCl, 10 mM Tris, 1 mM DTT and 5% glycerol, pH 7.4) as a series of sequential 50 ms 2D-data frames for a total exposure time of 1 s (Pilatus 2M photon counting detector). The resulting individual 50 ms 2D-frames underwent radial averaging to produce unsubtracted 1D $I(s)$ vs s scattering profiles [28]. Additional statistical checks were employed through the data reduction process so as not to include any sample (or buffer) frames affected by radiation damage (or systematic scaling errors) in the final, reduced 1D scattering profiles [29]. The scattering from the buffer was subtracted from the sample scattering to generate the final SAXS profile measured across an s-range of 0.013-3.8 nm^{-1}. From these data, several structural parameters were extracted using the ATSAS 2.8 software package [30]. First, the number of Shannon channels and maximum working s was assessed using *SHANUM* (Shannon channels = 14; s_{max} = 3.2 nm^{-1}: [31]). The extrapolated forward scattering intensity at zero angle, $I(0)$ and the radius of gyration R_g, were determined from both the Guinier approximation ($\ln I(s)$ vs s^2, in the s-range of $0.22 < sR_g < 1.3$, defining a working s_{min} of 0.07 nm^{-1}; [32]) and from the probable real-space distance distribution ($p(r)$ vs r profile) calculated from the indirect inverse Fourier transform of the data using *GNOM* [33]. The latter was also used to evaluate the maximum particle dimension, D_{max}. The molecular weight (MW) estimate of A1S_0222 was assessed using both concentration-dependent and concentration-independent methods. The concentration-independent MW methods included that of [34], the 'volume' of correlation, V_c, from [35] and the empirical correction to the Porod volume, V_p, as described in [36] as implemented in the respective ATSAS dattools *DATMOW*, *DATVC* and *DATPOROD*. The concentration-dependent MW estimate was performed relative to a bovine serum albumin (BSA) standard using the extrapolated $I(0)$ and the sample concentration (described in [37]). The final spatial representation of A1S_0222 – classified as compact using *DATCLASS* with an *AMBIMETER* shape ambiguity score of 0.9, i.e., as potentially unique [38] was obtained using *ab initio* bead modeling implemented in the program *DAMMIN* [39].

Ten individual bead models were generated that fit the data (assessed using the reduced χ^2 test and the Correlation Map, or CorMap, p-value. A χ^2 of 1 and $p > 0.01$ indicate no systematic discrepancies between the data-model fit [29]). The individual models were spatially aligned using *SUPCOMB* where the normalized spatial discrepancy (NSD) of the 10 model ensemble was assessed at 0.5 (aligned models with NSD < 1 are considered similar [40]). The models were subsequently averaged and bead occupancy-corrected using *DAMAVER* [41] and refined against the SAXS data using *DAMMIN*/*DAMSTART* to produce a final average 3D-spatial representation of A1S_0222 at an estimated resolution of 2.5 nm [42]. The SAXS data, $p(r)$ vs r profile, as well as the individual, averaged and refined DAMMIN models and the associated fits are deposited in the Small-angle Scattering Biological Data Bank with the accession code SASDD32 (SASBDB: www.sasbdb.org, [43]).

Structural homology modelling. Intensive Phyre2 modelling [44] was performed using the primary amino acid sequence of A1S_0222 as input to generate an atomistic 3D-homology model of A1S_0222. The fit to the SAXS data of the homology model as well as the fit to the data of the *E. coli* adenine-N6-DNA-methyltransferase, TaqI (Protein databank, PDB, accession 2ADM, chain A) were assessed using *CRYSOL* with 25 harmonics and a constant employed [45]. Additional normal mode structural refinement of the A1S_0222 homology model was performed using *SREFLEX* [46].

Phylogenetic profiling. We determined the presence absence pattern of orthologs to A1S_0222 across 1,548 *A. baumannii* strains, and 437 other taxa in the genus *Acinetobacter*. The ortholog search was performed in two stages. In stage one, we used the OMA algorithm [47] to compile an initial set of orthologous sequences from an all-against-all ortholog search in 104 representative *Acinetobacter* spp. representing all type strains. We then used this core orthologous group for a targeted ortholog search in the remaining taxa with HaMStR [48].

Results and Discussion

Motility assays. Preparing a library of *A. baumannii* ATCC 17978 mutants deficient in surface-associated motility, we found a knock out mutant of a putative DNA-(adenine N6)-methyltransferase, designated A1S_0222 in strain ATCC 17978. Figure

1 represents the motility deficiency of the A1S_0222 mutant in strain ATCC 17978. This A1S_0222-specfic motility deficiency could be confirmed in other *A. baumannii* strains, for instance DSM 30011 (data not shown) and 29D2 (data not shown; [49]).

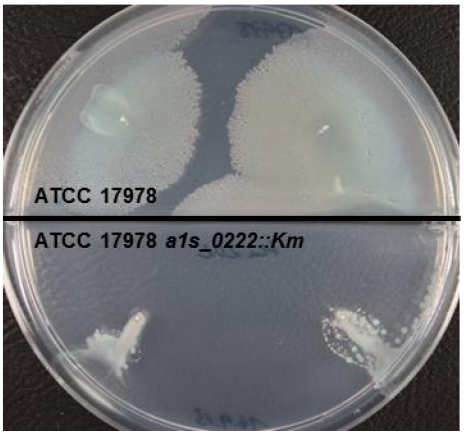

Fig. 1: The A1S_0222 mutant is deficient in surface-associated motility. *A. baumannii* ATCC 17978 (WT) and ATCC 17978 *a1s_0222::Km* (mutant) were inoculated on motility plates twice each and incubated for 16 h at 37°C. One representative picture is shown.

A1S_0222 protein overexpression and purification. To recombinantly produce the A1S_0222 protein, the *a1s_0222* gene was amplified by PCR and cloned into the expression vector pGEX-6P-3 designed for expression of glutathione S-transferase (GST)-fusion proteins. The plasmid insert was confirmed by DNA sequencing and transformed into *E. coli* BL21 (DE3) pLysS for expression. Preliminary experiments revealed that the best conditions for protein expression are the induction with 0.05 mM IPTG and the incubation at 20°C for 16 hours (data not shown). The GST-A1S_0222 fusion protein was purified from a 200 mL *E. coli* culture and the soluble lysate was loaded on a GSTPrep™ FF 16/10 column. Eluted fractions were pooled and GST tag was cleaved off by PreScission protease. The protein was further purified using HiTrap™ SP XL column (cation exchange chromatography, CEC) and subsequently high-salt buffer (430 mM NaCl) was changed into a low-salt buffer (150 mM NaCl) using a PD-10 column. The molecular weight of A1S_0222 is about 48 kDa. The protein then was concentrated to about 2.5 mg/mL with the best concentration results being achieved with a Hydrosart membrane (10,000 Da MWCO) although concentration of the protein remained inefficient. The purification of A1S_0222 is illustrated in Figure 2 and summarized in Table 1. We were able to purify A1S_0222 to near homogeneity.

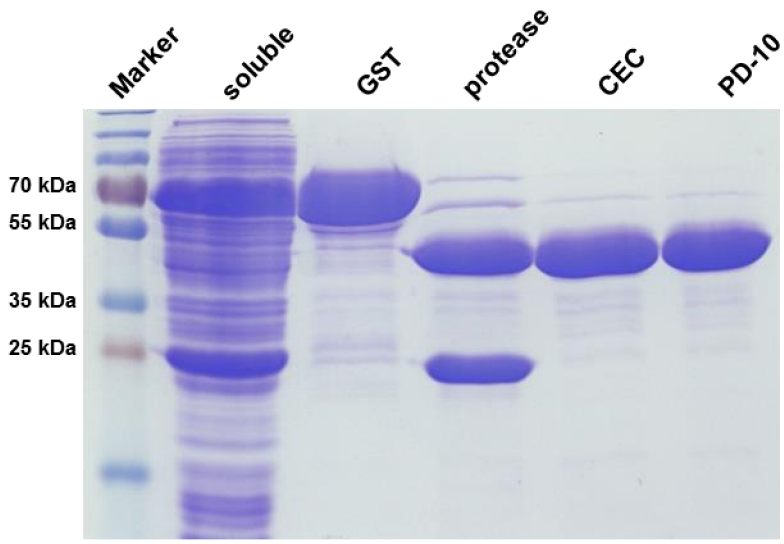

Fig. 2: Protein expression and purification of A1S_0222. Coomassie-stained SDS-PAGE showing the soluble fraction of the cell lysate after centrifugation ("soluble"), the fractions of GST-A1S_0222 after GST affinity chromatography ("GST"), cleavage of the GST-tag (26 kDa) after treatment with PreScission protease ("protease"), purified A1S_0222 (48 kDa) after cation exchange chromatography ("CEC") and after subsequent desalting using a PD-10 column ("PD-10").

Table 1: Purification of A1S_0222 recombinantly produced from a 200 mL *E. coli* culture

Purification step	Total volume [mL]	Protein conc. [mg/mL]	Total protein [mg]	Total A1S_0222 [mg]	Purity A1S_0222* [%]	Purification [fold]	Specific activity [mU/mg]
Soluble bacterial lysate	15	8.07	121.18	19.99	14.8	1	-
GSTPrep™	8	2.46	19.68	16,03	81.5	5.5	-
HiTrap™	4	2.41	9.64	9.29	96.4	6.5	-
PD-10	5	1.73	8.65	8.33	96.4[a]	6.5	-
Vivaspin® HY	1.5	2.46	3.69	3.55	96.4[b]	6.5	0.013

* Purity of A1S_0222 was determined by using ImageJ software and refers to GST-A1S_0222 (soluble bacterial lysate and GSTPrep™) and A1S_0222 without GST (HiTrap™; PD-10 and Vivaspin® HY), respectively.

[a] Due to background variation in the Coomassie-stained gel, the determined purity (with ImageJ) was adjusted to the purity of A1S_0222 after cation exchange chromatography (HiTrap™).

[b] A1S_0222 purity was comparable before and after concentration on Vivaspin® HY concentrators.

Identification of the A1S_0222 DNA recognition sequence and methyltransferase activity. According to REBASE, a database in which information about restriction enzymes, DNA methyltransferases, recognition and cleavage sites, published and unpublished references are collected [50, 51], the *A. baumannii* methyltransferase A1S_0222 was found to be annotated as M.AbaBGORF222P and M.Aba17978ORF8565P recognizing the RAATTY DNA sequence. DNA adenine methyltransferases, sharing the same recognition site as A1S_0222 were found in various bacteria including the MTase M.Hpy300III (GAATTC) from *Helicobacter pylori* isolate BCM-300 and M.Mpa1757II (GAATTC) from *Microcystis panniformis* FACHB-1757 (http://rebase.neb.com/rebase/rebase.html). Unfortunately most m6A methyltransferases in this database are not yet biochemically characterized. To detect the recognition site of A1S_0222, Sanger DNA sequencing was performed (Figure S1). In this automated dye terminator sequencing, m6A methylations in template DNA are identified by an increased complementary T signal [25]. As a consequence the recognition site of A1S_0222 was detected to be GAATTC in which the second adenine (underlined) gets methylated. This recognition sequence equates to the restriction site of the endonuclease EcoRI (G↓AATTC). As the next step we confirmed the enzymatic activity of the purified m6A methyltransferase A1S_0222. Therefore a methylation/restriction protection assay was established (Figure 3). A template-DNA (Int1), which contains only one A1S_0222 recognition site/EcoRI restriction site, was amplified by PCR. The purified PCR product Int1 was treated with A1S_0222 and afterwards incubated with and without EcoRI. As a control, Int1 was not treated with A1S_0222 but also incubated in the presence and absence of EcoRI. After incubation of Int1 with A1S_0222, EcoRI is no longer able to restrict the DNA Int1 (Figure 3, lane "+/+"), whereas Int1 gets restricted into 2 fragments without the A1S_0222 treatment (Figure 3, lane "-/+"). Thus, the results demonstrate the biological activity of the purified A1S_0222 as a DNA-(adenine N6)-methyltransferase. Note, that we did not observe any DNA degradation in this assay, demonstrating a DNase-free purification of A1S_0222. To address the specific activity of A1S_0222, a kinetic analysis of the methylation reaction was performed as described before. To this end, the methylation reaction was stopped and analyzed by

agarose gel electrophoresis after 10 min, 20 min, 30 min and 40 min (Figure 4). When incubating A1S_0222 for 10 min with 1 µg of DNA (Int1) half of the DNA was methylated and therefore protected from EcoRI restriction (lane "+/+", Figure 4). After 40 min 1 µg of DNA was completely methylated by A1S_0222 and could not be digested by EcoRI anymore. The specific activity of A1S_0222 was calculated to be approximately 0.013 mU/mg (Table 1). This low specific activity was confirmed using different DNA fragments (amplified from the *A. baumannii* 29D2 chromosome). One representative example is shown in Figure S2. In this case, about 80% of DNA is methylated by A1S_0222 after 40 minutes of incubation. The specific activity of 0.013 mU/mg for A1S_0222 is low compared to other orphan methyltransferases. For example, the most prominent *E. coli* DNA adenine methyltransferase, Dam, shows a specific activity of about 8.9 x10^5 U/mg [52]. As general proof of the suitability of the assay conditions, all tested DNA fragments were also treated with a commercial EcoRI methyltransferase from *E. coli* RY13 (New England BioLabs). Figures 4(B) and S2(B) illustrate that EcoRI methyltransferase confers full protection from EcoRI restriction within 30 seconds of incubation.

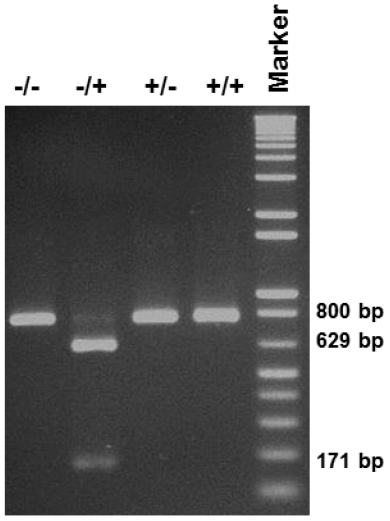

Fig. 3: Purified A1S_0222 protects DNA from EcoRI restriction. PCR-amplified DNA Int1 (800 bp) harboring a single EcoRI restriction site (G↓AATTC) was used for testing the biological activity of the putative DNA-(adenine N6)-methyltransferase A1S_0222. Methylation reaction was performed for 1 h at 37°C in the presence of 160 µM S-adenosyl-L-methionine (SAM). Subsequently, A1S_0222 was inactivated at 95°C (5 min), DNA was purified and subjected to EcoRI restriction for 2 h at 37°C. In lane "-/-" Int1 DNA was neither treated with A1S_0222 nor with EcoRI. Lane "-/+"

indicates the absence of A1S_0222 but the treatment of Int1 with EcoRI which results in cleavage of Int1 into two fragments (629 bp and 171 bp). Incubation of Int1 with A1S_0222 but no subsequent treatment with EcoRI is indicated by "+/-". Lane "+/+" indicates incubation of Int1 with A1S_0222 and subsequent treatment with EcoRI suggesting that methylation of Int1 by A1S_0222 protects the DNA against EcoRI digestion.

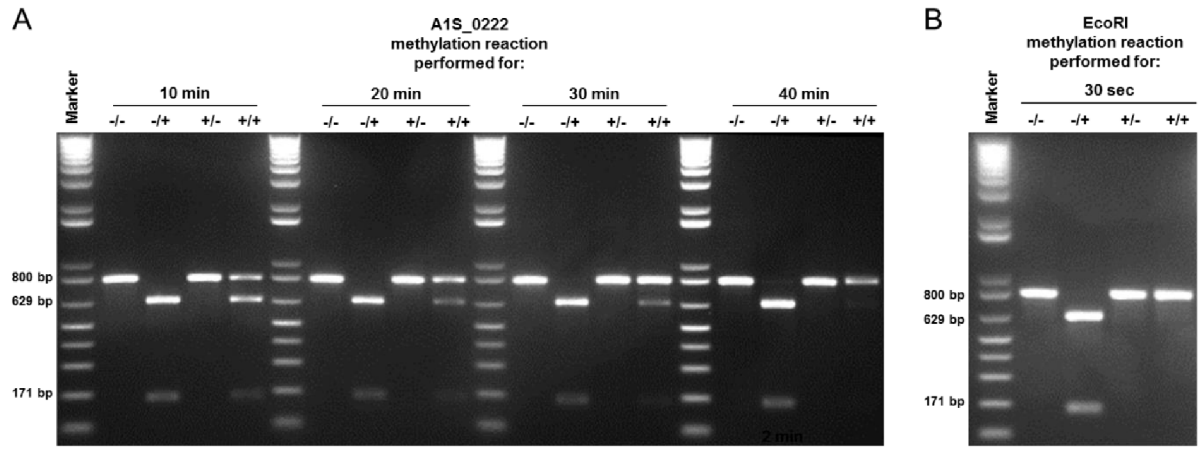

Fig. 4: Kinetic analysis of the A1S_0222 methylation reaction (A) and comparison to activity of EcoRI methyltransferase from *E. coli* RY13 (B). 1 µg of DNA (Int1) was used for methylation assay as described in legend to Fig. 3. Untreated Int1 is indicated by "-/-". DNA (Int1) not treated with A1S_0222 (7.38 µg) or EcoRI methyltransferase (40 U) but treated with EcoRI endonuclease is shown by "-/+". Int1 incubated with A1S_0222 or EcoRI methyltransferase but without *EcoR*I endonuclease treatment is indicated by "+/-". Int1 treated with A1S_0222 and subsequently treated with EcoRI endonuclease is shown by "+/+". **A.** After 10 minutes of treatment with A1S_0222, 0.5 µg of DNA (50%) is protected from restriction and after 40 minutes of incubation 1 µg DNA is almost completely methylated by A1S_0222. **B.** After 30 seconds of treatment of the Int1 DNA with EcoRI methyltransferase, all DNA (1 µg) is methylated and consequently protected from restriction by EcoRI endonuclease.

Structural characterization of A1S_0222. Given the low specific activity of our protein preparations and the considerable problems to concentrate the protein to levels above 2.5 mg/mL, we employed SAXS to structurally characterize and

generate a low-resolution model of A1S_0222 in solution. Figure 5 and Table 2 summarize the SAXS results which demonstrate that the protein is monomeric. Both concentration-dependent MW (52 kDa) and concentration-independent MW estimates (45-60 kDa) are in the range of the expected MW calculated from the amino acid sequence for the monomer (49 kDa). The shape classification of the data and the resulting $p(r)$ vs r profile indicate that A1S_0222 forms a compact, slightly anisotropic structure with an R_g of ~3 nm, with a D_{max} of ~11 nm (Table 2). The consensus low-resolution (2.5 nm) *DAMMIN* bead model (χ^2 = 1.06; CorMap p = 0.13) shows that A1S_0222 is flattened in one dimension, with possible structural extensions from the predominantly compact core (refer to SASBDB entry SASDD32). Of interest, a simple search of the PDB for DNA methyltransferases and the subsequent fitting the atomic structure of the *E.coli* adenine-N6-DNA-methyltransferase, TaqI (PDB 2ADM chain A; [53]) to the SAXS data suggests that TaqI and A1S_0222 may share structural features in common (Figure 6). Although the TaqI structure does not fit the SAXS data (χ^2 = 2.5, CorMap p = 0), the modelled intensities of the TaqI methyltransferase are not totally dissimilar across the experimental A1S_0222 SAXS profile which is surprising considering the two proteins only share 17 % amino acid sequence identity. Indeed subsequent Phyre2 homology modelling of A1S_0222, using the amino acid sequence of the protein as a template, consistently identified a number (more than 20) of high-scoring homologous fragments in the PDB (with greater than 97% confidence) that are categorized as DNA methyltransferases. The top-scoring homologues identified during the Phyre2 modelling are that of *E. coli* DNA adenine methyltransferase, PDB 2G1P (chain B) and bacteriophage T4 DNA adenine methyltransferase, PDB 1YF3 (chain A). As with TaqI, the final A1S_0222 Phyre2 homology model shows significant statistical discrepancies when fitting the model to the SAXS data (χ^2 = 2.6; CorMap p = 0). However, if the Phyre2 A1S_0222 homology model undergoes additional normal mode rigid-body refinement – that allows for subtle shifts in domain orientation – the predicted structure effectively ‘opens up’ and undergoes an overall extension to subsequently fit the SAXS data (χ^2 = 1.2; CorMap p = 0.019, Figure 6).

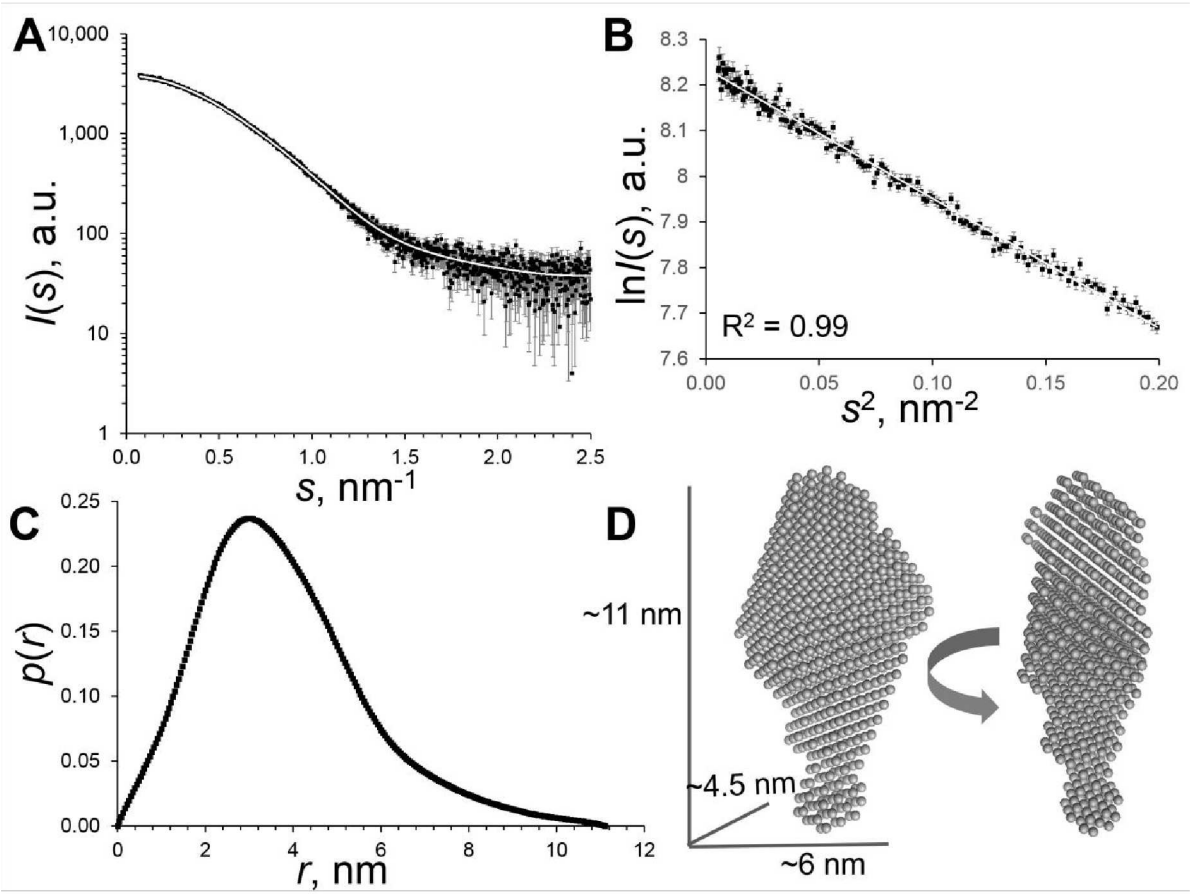

405

406 **Fig. 5: SAXS data and modelling. A.** SAXS data measured from A1S_0222 used to
407 calculate $p(r)$ vs r and for subsequent *ab initio* modelling (encompassing 10 out of 14
408 total Shannon channels; s_{min}, 0.07 nm^{-1}; s_{max}, 2.5 nm). **B.** The corresponding Guinier
409 plot and linear fit (white line; $R^2 = 0.99$) determined in the range $0.22 < sR_g < 1.3$. **C.**
410 The corresponding probable real space distance distribution, $p(r)$ vs r, calculated
411 from the inverse indirect Fourier transform of the data (reciprocal space fit to the
412 SAXS data: $\chi^2 = 1.08$, CorMap p = 0.16). **D.** An individually refined low-resolution
413 (2.5 nm) DAMMIN bead model of A1S_0222 derived from refining the averaged
414 superposition of 10 individual structures showing the shape and overall dimensions
415 of the protein in solution. The fit of the model to the SAXS data is shown in panel A
416 ($\chi^2 = 1.06$, CorMap p = 0.13). Additional details can be located in the SASBDB entry
417 SASDD32 (www.sasbdb.org).

418

419

420

Table 2: A1S_0222 SAXS structural parameters and modelling summary

Guinier Analysis		
$I(0)$ (error)	3766 a.u.	(+/- 7)
R_g (error)	2.9 nm	(+/- 0.3 nm)
qR_g range	$0.22 < sR_g < 1.3$	
***p*(*r*) analysis**		
$I(0)$ (error)	3773 a.u.	(+/- 8)
R_g (error)	3 nm	(+/- 0.01)
D_{max}	11 nm	
q range	0.07—2.5 nm^{-1}	
Reciprocal space fit: χ^2, CorMap p-value	$\chi^2 = 1.08$	p = 0.16
Porod volume, V_p	96 nm^3	
MW from $I(0)$ and concentration (ratio to expected value, 49 kDa)	53 kDa	(1.08)
Concentration independent MW estimates		
From V_p (Petoukhov et al 2012)	60 kDa	
From Fischer et al (2010)	48 kDa	
From Vc (Rambo and Tainer, 2013)	45 kDa	
Shape Classification (*DATCLASS*)*	compact	
Ab initio modelling		
Symmetry	P1	
Ambiguity measure(s) (*AMBIMETER*)	0.9	Potetially unique
Model fit χ^2, CorMap p-value	$\chi^2 = 1.06$	p = 0.13
Model volume and *MW* from DAM model	120 nm^3	60 kDa
Model resolution*	2.5 nm	

* *DATCLASS* is part of the ATSAS 2.8 suite of analytical dattools. ** The model resolution was obtained via the spatial alignment of ten individual *ab initio* models as per the method of Tuukkanen *et al.* 2016 [42].

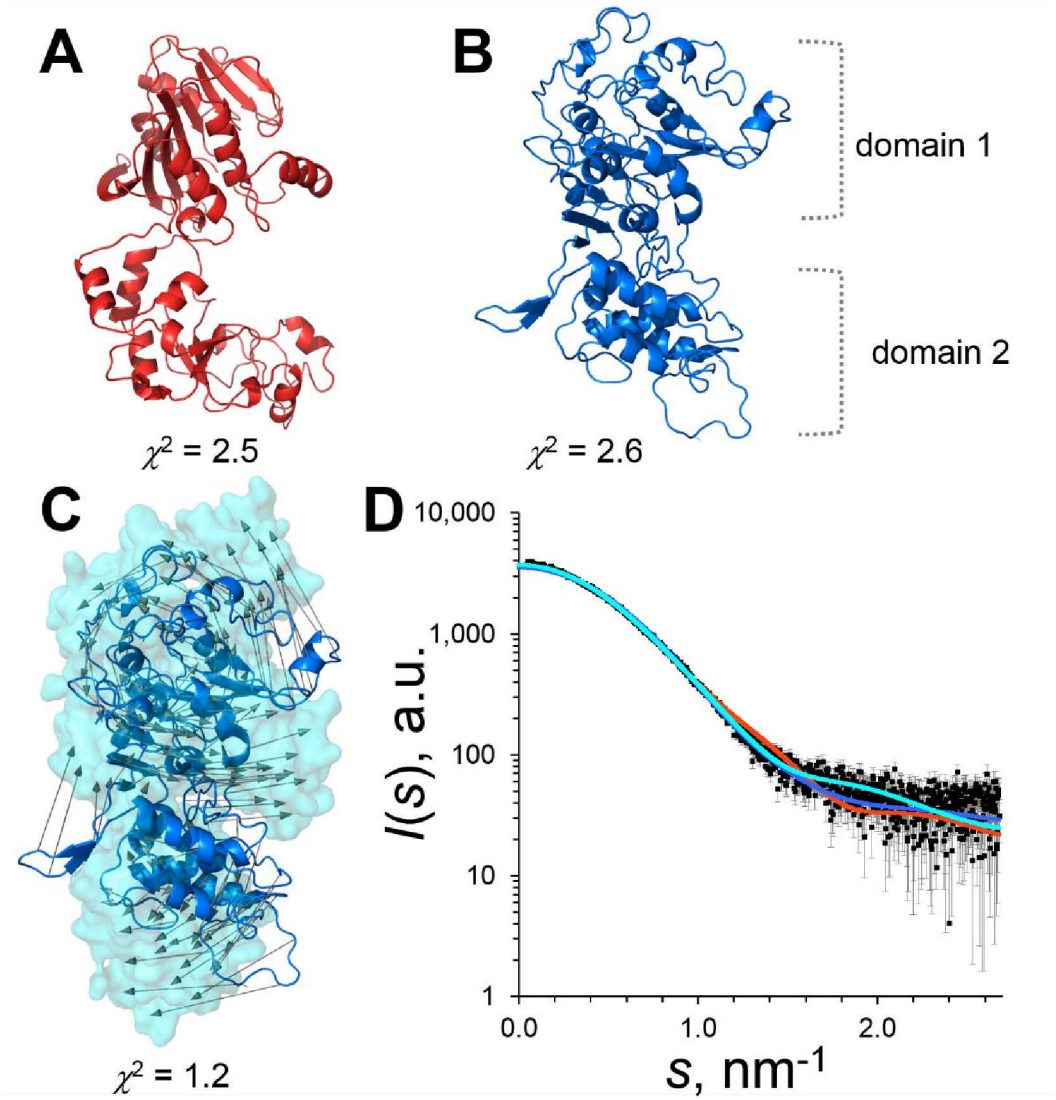

426

427 **Fig. 6: Adenine-N6-DNA-methyltransferase models. A.** The structural
428 representation of the *E. coli* adenine-N6-DNA-methyltransferase, TaqI (PDB: 2ADM,
429 chain A; red ribbon) and the reported χ^2 discrepancy of the model-fit to the A1S_0222
430 SAXS data. **B.** The predicted Phyre2 homology model of A1S_0222 (blue ribbon)
431 constructed from homologous DNA methyltransferase structural templates. Although
432 the enzyme is predicted to have two major domains, in the relative spatial
433 orientations depicted here, the fit to the SAXS data remains poor. **C.** A significant
434 improvement in the fit to the SAXS data for the Phyre2 homology model occurs if the
435 predicted domains of A1S_0222 shift orientation with respect to each other, i.e.,
436 rotate/move apart (grey arrows) to form a more extended structure (cyan surface).
437 **D.** The corresponding fits to the SAXS data of the modelled scattering intensities of
438 TaqI (red), the Phyre2 homology model (blue) and the Phyre2 A1S_0222 structure
439 that has undergone a shift in the domain orientations (cyan).

The phylogenetic relationship of A1S_0222 to other *Acinetobacter* orphan DNA methyltransferases. Lastly, we analyzed the phylogenetic distribution of A1S_0222 within *Acinetobacter* spp. Our analysis revealed that this protein is encoded in all but 19 of the 1,985 genomes covering the full known diversity of the genus *Acinetobacter*. The 19 cases where no ortholog could be identified are shown in Table 3. We see no obvious grouping of individual species where this gene is missing. Instead, we conclude that this protein is ubiquitously present in *Acinetobacter* spp.. Most probably, issues connected to data quality and the draft status of most *Acinetobacter* spp. genome reconstructions explain the few cases where no ortholog could be detected.

Table 3: *Acinetobacter* spp. lacking an ortholog to A1S_0222

Assembly name	NCBI ID	Taxon name
GCF_000805035.1	470	*Acinetobacter baumannii*
GCF_000939415.2	470	*Acinetobacter baumannii*
GCF_001415065.1	470	*Acinetobacter baumannii*
GCF_001416235.1	470	*Acinetobacter baumannii*
GCA_001510805.1	471	*Acinetobacter calcoaceticus GK2*
GCF_000962795.1	134533	*Acinetobacter parvus*
GCA_900096915.1	281376	*Acinetobacter seohaensis*
GCA_900107285.1	595670	*Acinetobacter kyonggiensis*
GCF_000368825.1	981336	*Acinetobacter ursingii DSM 16037*
GCA_000803285.1	1148157	*Acinetobacter oleivorans*
GCA_900096955.1	1219383	*Acinetobacter boissieri*
GCA_900096895.1	1226327	*Acinetobacter kookii*
GCA_000433235.1	1262690	*Acinetobacter sp. CAG:196*
GCF_000581675.1	1310582	*Acinetobacter baumannii 662545-1347*
GCA_900095025.1	1673609	*Acinetobacter albensis*
GCA_001767535.1	1797234	*Acinetobacter sp. GWC1_38_13*
GCA_001768625.1	1797235	*Acinetobacter sp. RIFCSPHIGHO2_12_41_5*
GCA_001581975.1	1809055	*Acinetobacter sp. DUT-2*
GCA_001720685.1	1856846	*Acinetobacter sp. 51m*

Conclusion

In conclusion, we confirmed the classification of A1S_0222 as a Type II N6-adenine DNA methyltransferase recognizing GAATTC in line with the REBASE *in silico* classification [51]. A1S_0222 seems to act as an orphan methyltransferase since no evidence for an associated endonuclease could be found in REBASE. We propose the name AamA (*Acinetobacter* adenine methyltransferase A) in addition to the formal names M.AbaBGORF222P and M.Aba17978ORF8565P provided by REBASE. To the best of our knowledge, this is the first DNA methyltransferase of the nosocomial pathogen *A. baumannii* that has been experimentally studied.

Acknowledgements

This project was funded by the Deutsche Forschungsgemeinschaft (DFG) within FOR 2251 (project grants EB 285/2-1 and WI 3272/3-1) and in part by additional contributions from the Bundesministerium für Bildung und Forschung (D.I.S award Nos. BIOSCAT [05K12YE1]) and the Horizon 2020 programme of the European Union, iNEXT [653706; D.I.S].

References

[1] M. Eveillard, M. Kempf, O. Belmonte, H. Pailhories, M.L. Joly-Guillou, Reservoirs of *Acinetobacter baumannii* outside the hospital and potential involvement in emerging human community-acquired infections. Int J Infect Dis 17 (2013) e802-805.

[2] M.J. McConnell, L. Actis, J. Pachon, *Acinetobacter baumannii*: human infections, factors contributing to pathogenesis and animal models. FEMS Microbiol Rev 37 (2013) 130-155.

[3] J.H. Baang, P. Axelrod, B.K. Decker, A.M. Hujer, G. Dash, A.R. Truant, R.A. Bonomo, T. Fekete, Longitudinal epidemiology of multidrug-resistant (MDR) *Acinetobacter* species in a tertiary care hospital. Am J Infect Control 40 (2012) 134-137.

[4] E. Tacconelli, E. Carrara, A. Savoldi, S. Harbarth, M. Mendelson, D.L. Monnet, C. Pulcini, G. Kahlmeter, J. Kluytmans, Y. Carmeli, M. Ouellette, K. Outterson, J.

Patel, M. Cavaleri, E.M. Cox, C.R. Houchens, M.L. Grayson, P. Hansen, N. Singh, U. Theuretzbacher, N. Magrini, W.H.O.P.P.L.W. Group, Discovery, research, and development of new antibiotics: the WHO priority list of antibiotic-resistant bacteria and tuberculosis. Lancet Infect Dis (2017).

[5] J. Henrichsen, J. Blom, Correlation between twitching motility and possession of polar fimbriae in *Acinetobacter calcoaceticus*. Acta Pathol Microbiol Scand B 83 (1975) 103-115.

[6] J. Henrichsen, The influence of changes in the environment on twitching motility. Acta Pathol Microbiol Scand B 83 (1975) 179-186.

[7] C.M. Harding, E.N. Tracy, M.D. Carruthers, P.N. Rather, L.A. Actis, R.S. Munson, Jr., *Acinetobacter baumannii* strain M2 produces type IV pili which play a role in natural transformation and twitching motility but not surface-associated motility. MBio 4 (2013).

[8] G. Wilharm, J. Piesker, M. Laue, E. Skiebe, DNA uptake by the nosocomial pathogen *Acinetobacter baumannii* occurs during movement along wet surfaces. J Bacteriol 195 (2013) 4146-4153.

[9] J.S. Mattick, Type IV pili and twitching motility. Annu Rev Microbiol 56 (2002) 289-314.

[10] K.M. Clemmer, R.A. Bonomo, P.N. Rather, Genetic analysis of surface motility in *Acinetobacter baumannii*. Microbiology 157 (2011) 2534-2544.

[11] E. Skiebe, V. de Berardinis, P. Morczinek, T. Kerrinnes, F. Faber, D. Lepka, B. Hammer, O. Zimmermann, S. Ziesing, T.A. Wichelhaus, Surface-associated motility, a common trait of clinical isolates of *Acinetobacter baumannii*, depends on 1, 3-diaminopropane. International Journal of Medical Microbiology 302 (2012) 117-128.

[12] A.C. Jacobs, C.E. Blanchard, S.C. Catherman, P.M. Dunman, Y. Murata, An ribonuclease T2 family protein modulates *Acinetobacter baumannii* abiotic surface colonization. PLoS One 9 (2014) e85729.

[13] K.A. Tipton, P.N. Rather, An ompR/envZ Two-Component System Ortholog Regulates Phase Variation, Osmotic Tolerance, Motility, and Virulence in *Acinetobacter baumannii* strain AB5075. J Bacteriol (2016).

[14] J. Collier, Epigenetic regulation of the bacterial cell cycle. Curr Opin Microbiol 12 (2009) 722-729.

[15] A. Bart, M. Van Passel, K. Van Amsterdam, A. Van Der Ende, Direct detection of methylation in genomic DNA. Nucleic acids research 33 (2005) e124-e124.

[16] X. Cheng, Structure and function of DNA methyltransferases. Annual review of biophysics and biomolecular structure 24 (1995) 293-318.
[17] D. Wion, J. Casadesus, N6-methyl-adenine: an epigenetic signal for DNA-protein interactions. Nat Rev Microbiol 4 (2006) 183-192.
[18] S. Adhikari, P.D. Curtis, DNA methyltransferases and epigenetic regulation in bacteria. FEMS Microbiol Rev 40 (2016) 575-591.
[19] T.A. Bickle, D.H. Kruger, Biology of DNA restriction. Microbiol Rev 57 (1993) 434-450.
[20] M.G. Marinus, N.R. Morris, Isolation of deoxyribonucleic acid methylase mutants of *Escherichia coli* K-12. J Bacteriol 114 (1973) 1143-1150.
[21] J.E. Brooks, R.M. Blumenthal, T.R. Gingeras, The isolation and characterization of the *Escherichia coli* DNA adenine methylase (*dam*) gene. Nucleic Acids Res 11 (1983) 837-851.
[22] G. Badie, D.M. Heithoff, R.L. Sinsheimer, M.J. Mahan, Altered levels of Salmonella DNA adenine methylase are associated with defects in gene expression, motility, flagellar synthesis, and bile resistance in the pathogenic strain 14028 but not in the laboratory strain LT2. J Bacteriol 189 (2007) 1556-1564.
[23] S. Falker, J. Schilling, M.A. Schmidt, G. Heusipp, Overproduction of DNA adenine methyltransferase alters motility, invasion, and the lipopolysaccharide O-antigen composition of *Yersinia enterocolitica*. Infect Immun 75 (2007) 4990-4997.
[24] K.H. Choi, A. Kumar, H.P. Schweizer, A 10-min method for preparation of highly electrocompetent *Pseudomonas aeruginosa* cells: application for DNA fragment transfer between chromosomes and plasmid transformation. J Microbiol Methods 64 (2006) 391-397.
[25] B.S. Rao, A. Buckler-White, Direct visualization of site-specific and strand-specific DNA methylation patterns in automated DNA sequencing data. Nucleic Acids Res 26 (1998) 2505-2507.
[26] C.E. Blanchet, A. Spilotros, F. Schwemmer, M.A. Graewert, A. Kikhney, C.M. Jeffries, D. Franke, D. Mark, R. Zengerle, F. Cipriani, S. Fiedler, M. Roessle, D.I. Svergun, Versatile sample environments and automation for biological solution X-ray scattering experiments at the P12 beamline (PETRA III, DESY). J Appl Crystallogr 48 (2015) 431-443.
[27] A. Round, F. Felisaz, L. Fodinger, A. Gobbo, J. Huet, C. Villard, C.E. Blanchet, P. Pernot, S. McSweeney, M. Roessle, D.I. Svergun, F. Cipriani, BioSAXS Sample

554 Changer: a robotic sample changer for rapid and reliable high-throughput X-ray
555 solution scattering experiments. Acta Crystallogr D Biol Crystallogr 71 (2015) 67-75.
556 [28] D. Franke, A.G. Kikhney, D.I. Svergun, Automated acquisition and analysis of
557 small angle X-ray scattering data. Nuclear Instruments and Methods in Physics
558 Research Section A: Accelerators, Spectrometers, Detectors and Associated
559 Equipment 689 (2012) 52-59.
560 [29] D. Franke, C.M. Jeffries, D.I. Svergun, Correlation Map, a goodness-of-fit test
561 for one-dimensional X-ray scattering spectra. Nat Methods 12 (2015) 419-422.
562 [30] D. Franke, M.V. Petoukhov, P.V. Konarev, A. Panjkovich, A. Tuukkanen,
563 H.D.T. Mertens, A.G. Kikhney, N.R. Hajizadeh, J.M. Franklin, C.M. Jeffries, D.I.
564 Svergun, ATSAS 2.8: a comprehensive data analysis suite for small-angle scattering
565 from macromolecular solutions. J Appl Crystallogr 50 (2017) 1212-1225.
566 [31] P.V. Konarev, D.I. Svergun, A posteriori determination of the useful data range
567 for small-angle scattering experiments on dilute monodisperse systems. IUCrJ 2
568 (2015) 352-360.
569 [32] A. Guinier, La diffraction des rayons X aux très petits angles : application à
570 l'étude de phénomènes ultramicroscopiques. Ann Phys 11 (1939) 161-237.
571 [33] D. Svergun, Determination of the regularization parameter in indirect-transform
572 methods using perceptual criteria. Journal of Applied Crystallography 25 (1992) 495-
573 503.
574 [34] H. Fischer, M. de Oliveira Neto, H.B. Napolitano, I. Polikarpov, A.F. Craievich,
575 Determination of the molecular weight of proteins in solution from a single small-
576 angle X-ray scattering measurement on a relative scale. Journal of Applied
577 Crystallography 43 (2010) 101-109.
578 [35] R.P. Rambo, J.A. Tainer, Accurate assessment of mass, models and
579 resolution by small-angle scattering. Nature 496 (2013) 477-481.
580 [36] M.V. Petoukhov, D. Franke, A.V. Shkumatov, G. Tria, A.G. Kikhney, M. Gajda,
581 C. Gorba, H.D. Mertens, P.V. Konarev, D.I. Svergun, New developments in the
582 ATSAS program package for small-angle scattering data analysis. J Appl Crystallogr
583 45 (2012) 342-350.
584 [37] C.M. Jeffries, M.A. Graewert, C.E. Blanchet, D.B. Langley, A.E. Whitten, D.I.
585 Svergun, Preparing monodisperse macromolecular samples for successful biological
586 small-angle X-ray and neutron-scattering experiments. Nat Protoc 11 (2016) 2122-
587 2153.

588 [38] M.V. Petoukhov, D.I. Svergun, Ambiguity assessment of small-angle
589 scattering curves from monodisperse systems. Acta Crystallogr D Biol Crystallogr 71
590 (2015) 1051-1058.
591 [39] D.I. Svergun, Restoring low resolution structure of biological macromolecules
592 from solution scattering using simulated annealing. Biophys J 76 (1999) 2879-2886.
593 [40] M.B. Kozin, D.I. Svergun, Automated matching of high- and low-resolution
594 structural models. Journal of Applied Crystallography 34 (2001) 33-41.
595 [41] V.V. Volkov, D.I. Svergun, Uniqueness of ab initio shape determination in
596 small-angle scattering. Journal of Applied Crystallography 36 (2003) 860-864.
597 [42] A.T. Tuukkanen, G.J. Kleywegt, D.I. Svergun, Resolution of ab initio shapes
598 determined from small-angle scattering. IUCrJ 3 (2016) 440-447.
599 [43] E. Valentini, A.G. Kikhney, G. Previtali, C.M. Jeffries, D.I. Svergun, SASBDB,
600 a repository for biological small-angle scattering data. Nucleic Acids Res 43 (2015)
601 D357-363.
602 [44] L.A. Kelley, S. Mezulis, C.M. Yates, M.N. Wass, M.J. Sternberg, The Phyre2
603 web portal for protein modeling, prediction and analysis. Nat Protoc 10 (2015) 845-
604 858.
605 [45] D. Svergun, C. Barberato, M.H.J. Koch, CRYSOL - a Program to Evaluate X-
606 ray Solution Scattering of Biological Macromolecules from Atomic Coordinates.
607 Journal of Applied Crystallography 28 (1995) 768-773.
608 [46] A. Panjkovich, D.I. Svergun, Deciphering conformational transitions of proteins
609 by small angle X-ray scattering and normal mode analysis. Phys Chem Chem Phys
610 18 (2016) 5707-5719.
611 [47] A.C. Roth, G.H. Gonnet, C. Dessimoz, Algorithm of OMA for large-scale
612 orthology inference. BMC Bioinformatics 9 (2008) 518.
613 [48] I. Ebersberger, S. Strauss, A. von Haeseler, HaMStR: profile hidden markov
614 model based search for orthologs in ESTs. BMC Evol Biol 9 (2009) 157.
615 [49] G. Wilharm, E. Skiebe, P.G. Higgins, M.T. Poppel, U. Blaschke, S. Leser, C.
616 Heider, M. Heindorf, P. Brauner, U. Jackel, K. Bohland, C. Cuny, A. Lopinska, P.
617 Kaminski, M. Kasprzak, M. Bochenski, O. Ciebiera, M. Tobolka, K.M. Zolnierowicz, J.
618 Siekiera, H. Seifert, S. Gagne, S.P. Salcedo, M. Kaatz, F. Layer, J.K. Bender, S.
619 Fuchs, T. Semmler, Y. Pfeifer, L. Jerzak, Relatedness of wildlife and livestock avian
620 isolates of the nosocomial pathogen *Acinetobacter baumannii* to lineages spread in
621 hospitals worldwide. Environ Microbiol 19 (2017) 4349-4364.

[50] R.J. Roberts, T. Vincze, J. Posfai, D. Macelis, REBASE: restriction enzymes and methyltransferases. Nucleic Acids Res 31 (2003) 418-420.

[51] R.J. Roberts, T. Vincze, J. Posfai, D. Macelis, REBASE--a database for DNA restriction and modification: enzymes, genes and genomes. Nucleic Acids Res 43 (2015) D298-299.

[52] S. Urig, H. Gowher, A. Hermann, C. Beck, M. Fatemi, A. Humeny, A. Jeltsch, The *Escherichia coli* dam DNA methyltransferase modifies DNA in a highly processive reaction. J Mol Biol 319 (2002) 1085-1096.

[53] G. Schluckebier, M. Kozak, N. Bleimling, E. Weinhold, W. Saenger, Differential binding of S-adenosylmethionine S-adenosylhomocysteine and Sinefungin to the adenine-specific DNA methyltransferase M.TaqI. J Mol Biol 265 (1997) 56-67.

Supplementary material

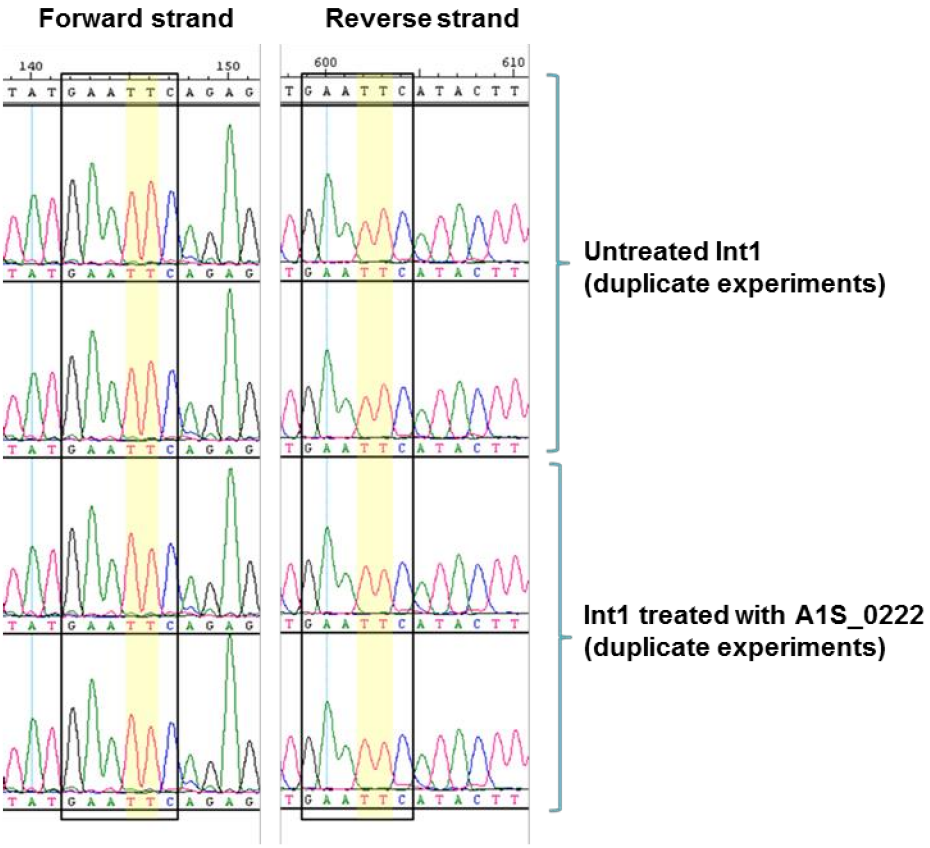

Fig. S1: Sanger DNA sequencing indicates A1S_0222-dependent methylation of adenine within a GAATTC recognition site. In this automated dye terminator sequencing an m6A methylation in template DNA is indicated by an increased complementary T signal in the DNA sequence [25]. After an m6A methylation the T-peak pattern changes to an increase of the first T-peak and a lower second T-peak right after the methylated adenine. Details of sequencing chromatograms with the putative recognition site GAATTC boxed. In non-treated DNA the first T-peaks are lower compared to the second T-peaks on forward and reverse strand (yellow box). Upon treatment of Int1 DNA with purified A1S_0222 the first T-peak intensifies on both strands whereas the second T-peak attenuates. This suggests the recognition site of A1S_0222 to be GAATTC and the second adenine (underlined) to be methylated.

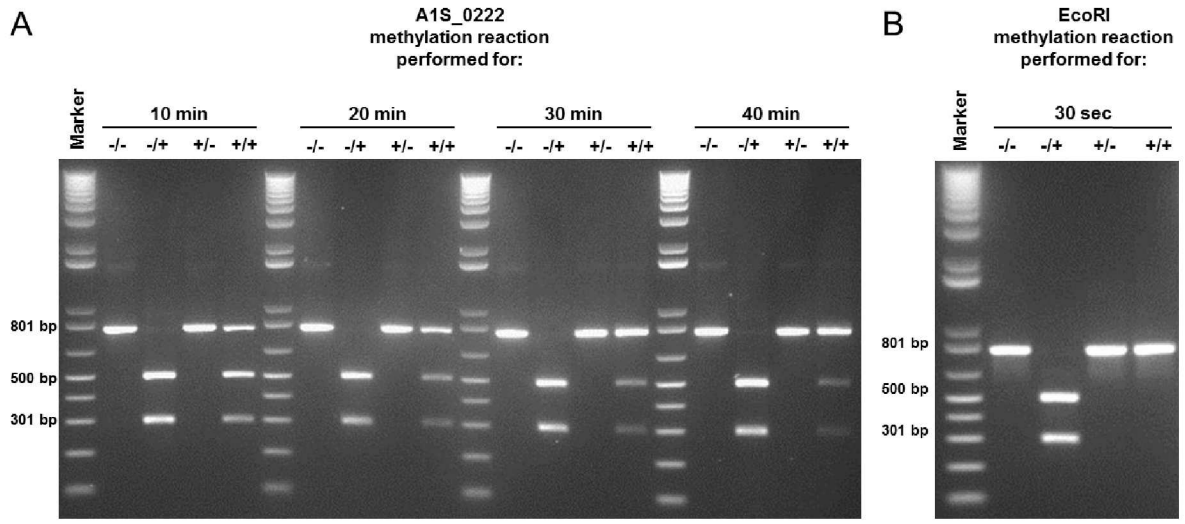

Fig. S2: Kinetic analysis of the A1S_0222 methylation reaction (A) and comparison to activity of EcoRI methyltransferase (from *E. coli* RY13) (B). For the methylation assay 1 µg of DNA (Seq3) was used. Untreated Seq3 is indicated by "-/-". DNA (Seq3) not treated with A1S_0222 (7.38 µg) or EcoRI methyltransferase (40U), but treated with EcoRI endonuclease is shown by "-/+". Seq3 incubated with A1S_0222 or EcoRI methyltransferase, but without EcoRI endonuclease treatment is indicated by "+/-". Seq3 treated with A1S_0222 or EcoRI methyltransferase and subsequently treated with EcoRI endonuclease is shown by "+/+". **A.** 10 minutes after incubation with A1S_0222 about 30% of DNA is protected from restriction. After 40 minutes of incubation about 80% of DNA is methylated by A1S_0222. **B.** After 30 seconds of incubation with EcoRI methyltransferase, 1 µg of DNA is completely protected from restriction by EcoRI endonuclease.